

Computational Analysis on the Allostery of Tryptophan Synthase: Relationship between α/β -Ligand Binding and Distal Domain Closure

Shingo Ito, Kiyoshi Yagi, and Yuji Sugita*



Cite This: *J. Phys. Chem. B* 2022, 126, 3300–3308



Read Online

ACCESS |



Metrics & More

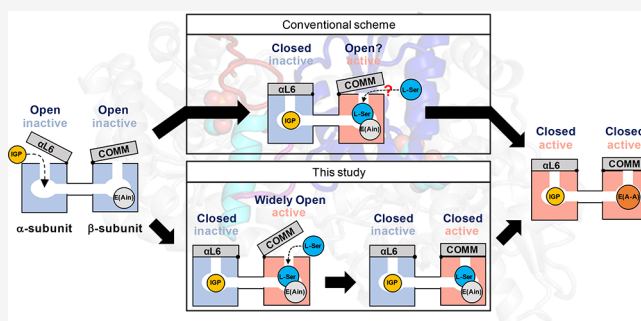


Article Recommendations



Supporting Information

ABSTRACT: Tryptophan synthase (TRPS) is a bifunctional enzyme consisting of α and β -subunits and catalyzes the last two steps of L-tryptophan (L-Trp) biosynthesis, namely, cleavage of 3-indole-D-glycerol-3'-phosphate (IGP) into indole and glyceraldehyde-3-phosphate (G3P) in the α -subunit, and a pyridoxal phosphate (PLP)-dependent reaction of indole and L-serine (L-Ser) to produce L-Trp in the β -subunit. Importantly, the IGP binding at the α -subunit affects the β -subunit conformation and its ligand-binding affinity, which, in turn, enhances the enzymatic reaction at the α -subunit. The intersubunit communications in TRPS have been investigated extensively for decades because of the fundamental and pharmaceutical importance, while it is still difficult to answer how TRPS allostery is regulated at the atomic detail. Here, we investigate the allosteric regulation of TRPS by all-atom classical molecular dynamics (MD) simulations and analyze the potential of mean-force (PMF) along conformational changes of the α - and β -subunits. The present simulation has revealed a widely opened conformation of the β -subunit, which provides a pathway for L-Ser to enter into the β -active site. The IGP binding closes the α -subunit and induces a wide opening of the β -subunit, thereby enhancing the binding affinity of L-Ser to the β -subunit. Structural analyses have identified critical hydrogen bonds (HBs) at the interface of the two subunits (α G181- β S178, α P57- β R175, etc.) and HBs between the β -subunit (β T110 – β H115) and a complex of PLP and L-Ser (an α -aminoacrylate intermediate). The former HBs regulate the allosteric, β -subunit opening, whereas the latter HBs are essential for closing the β -subunit in a later step. The proposed mechanism for how the interdomain communication in TRPS is realized with ligand bindings is consistent with the previous experimental data, giving a general idea to interpret the allosteric regulations in multidomain proteins.



1. INTRODUCTION

The tryptophan (Trp) biosynthesis has recently drawn great attention as a potential target for anti-tuberculosis (TB) drugs.^{1,2} TB disease is one of the globally spread epidemics, where 1.3 million deaths have been estimated in 2021.³ Furthermore, the treatment of multidrug-resistant, pathogenic bacteria, *Mycobacterium tuberculosis* (*M.tb*), requires an urgent need for new therapeutic approaches with a novel molecular target. Tryptophan synthase (TRPS), which catalyzes the last two steps of Trp biosynthesis, is a bifunctional enzyme consisting of two subunits, α and β . One of the unique features of TRPS is an allosteric regulation, where conformational changes of the α - and β -subunits are synchronized with the activity of enzymatic reactions.^{4,5} Recent studies have reported effective allosteric inhibitors of TRPS that kills *M.tb*.^{6,7} Nonetheless, further understanding in an atomic detail is necessary for precise control of the allosteric inhibition.

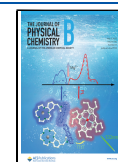
The structure and reaction of TRPS from *Salmonella typhimurium* have been extensively studied since the 1980s.^{8–10} The two subunits of TRPS have their own active

sites, which are called the α - and β -active sites. At the α -active site, the α -reaction cleaves 3-indole-D-glycerol-3'-phosphate (IGP) into indole and glyceraldehyde-3-phosphate (G3P). The indole is transferred to the β -active site through an internal tunnel of 25 Å length, preventing the leak of indole during the reaction cycle. At the β -active site, the β -reaction proceeds in two stages. First, the pyridoxal phosphate (PLP) co-factor, covalently bound to β K87 of the β -subunit [denoted E(Ain)], reacts with a ligand, L-serine (L-Ser), to produce an α -aminoacrylate [denoted E(A-A)]. In the second stage, E(A-A) reacts with the indole transferred from the α -active site to yield the final product, L-Trp. Interestingly, the α and β -reactions as well as the indole transfer are functionally coupled

Received: March 4, 2022

Revised: April 4, 2022

Published: April 21, 2022



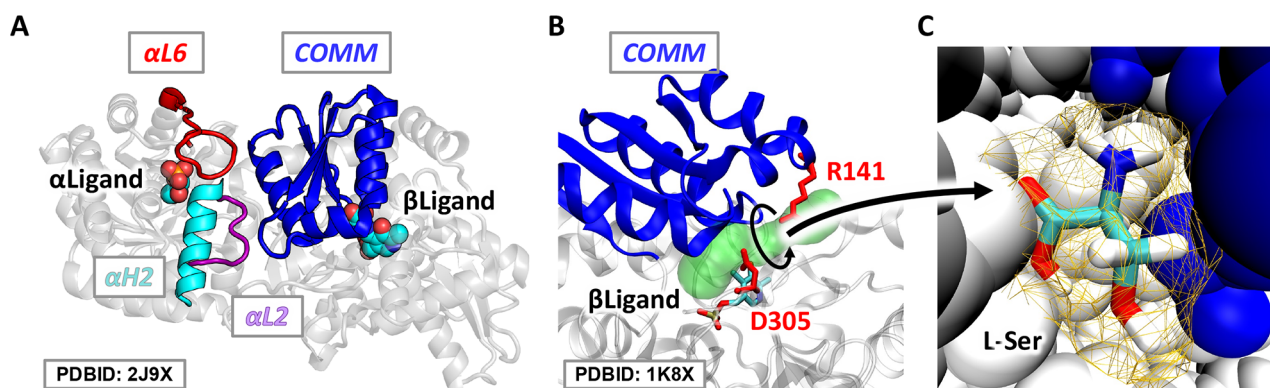


Figure 1. (A) Essential domains related to the allostery of TRPS located at the interface of α and β -subunits: α L2 (purple, residue ID 53–60), α L6 (red, residue ID 176–192), α H2 (cyan, residue ID 61–75), and the COMM domain (blue, residue ID 102–189). (B) Entry pathway proposed from the X-ray crystal structures to the β -active site (green). (C) Bottleneck along the proposed L-Ser entry pathway. The white and blue vdW spheres represent the β -subunit and the COMM domain, respectively. The surface of the L-Ser (yellow colored wire) overlaps with the surface of TRPS (vdW sphere). Detailed information on how to set L-Ser in the pathway is described in the [Supporting Information](#).

to each other. (1) The binding of IGP at the α -active site enhances the affinity of L-Ser binding at the β -active site¹¹ and promotes the reaction of L-Ser and PLP to produce E(A-A).^{12,13} (2) The formation of E(A-A) promotes the cleavage of IGP, the indole transfer, and the production of L-Trp.^{12,13} The whole scheme of the Trp synthesis is schematically drawn in [Figure S1](#). The allosteric regulation has been extensively investigated by structural and kinetic studies combined with site-directed mutagenesis.^{14–24} These studies have revealed two important regions, a flexible loop 6 in the α -subunit (α L6) and a communication (COMM) domain in the β -subunit, which are located in the proximity of the two active sites as shown in [Figure 1A](#). These regions not only serve as gates of the α - and β -active sites but also interact with each other at the interface of the two subunits. The hydrogen bond (HB) between α G181 in α L6 and β S178 in the COMM domain has been suggested to be critical for the ligand-induced conformational changes.^{25,26}

Despite accumulated structural and functional information of TRPS, there are still many questions to be answered regarding the allostery of TRPS. One of the most important questions is how IGP binding at the α -active site can enhance the ligand affinity at the distal β -active site. The entry pathway proposed from the X-ray crystal structures is too narrow for the L-Ser entry either in the ApoE(Ain) state (PDB ID: 1K8X²⁰) ([Figure 1B,C](#)) or in the IGPIE(Ain) state (PDB ID: 1WBJ²¹), suggesting the importance of dynamic structures of TRPS. Hereafter, we use the notation A|B, where A and B indicate the bound (and reaction) states of the α - and β -active site, respectively. After the β -subunit is widely opened for making sufficient space for the L-Ser entry, it should be closed for enhancing the reaction at the β -active site. Mechanisms for this domain closure also remain elusive. To answer these questions, dynamic structures of TRPS and interdomain interaction in different ligand-bound states are necessary in addition to the static X-ray crystal structures.

Molecular dynamics (MD) simulations of biomacromolecules have made great progress in the last decade.^{27–29} Developments of computational algorithms and MD-specialized supercomputers³⁰ have made feasible the simulation in a time scale of 100 μ s or even milliseconds. Enhanced sampling methods are another way to enable an efficient sampling of conformational space and the computation of free-energy landscapes of biomolecules.^{31–33} Replica-exchange molecular

dynamics (REMD),^{34–36} generalized replica exchange solute tempering (gREST),^{37,38} Gaussian accelerated MD (GaMD),³⁹ and metadynamics⁴⁰ are representative algorithms in enhanced sampling algorithms of biomolecular simulations. They are ready to use in most of MD software with/without additional tools, such as PLUMED.⁴¹ In our MD program GENESIS (<https://www.r-ccs.riken.jp/labs/cbrt/>),^{42,43} many enhanced sampling algorithms are available for users just by preparing input scripts.

Several important computational studies on TRPS have been reported in the literature.^{44–50} In a pioneering work by Fatmi et al.,⁴⁵ all-atom MD simulations of TRPS were performed in the apo and ligand-bound [with IGP and E(A-A)] states to clarify ligand-induced conformational changes of α L6 and the COMM domain, although the sampling was limited to a 60 ns conventional MD in those days. More recently, Maria-Solano et al.⁴⁸ studied the TRPS from *Pyrococcus furiosus* (Pf TrpS) by metadynamics simulations. The potential of mean force (PMF) was computed along the open-to-closed conformational changes of the COMM domain in various intermediates of the β -reaction to discuss the stability of Pf TrpS (α - and β -complex) and a stand-alone β -subunit with mutations. To the best of our knowledge, there are no computational studies on the allosteric regulation of the β -subunit motions induced by IGP binding at the α -subunit.

To reveal the molecular mechanisms for the allosteric structures of TRPS, we have carried out extensive MD simulations of TRPS in three different ligand-bound states, namely, ApoE(Ain), IGPIE(Ain), and IGPIE(A-A) bound states. The PMF in each state was computed using the umbrella sampling (US) method.⁵¹ The main finding in the simulation is that the COMM domain takes a stable, widely open form upon the IGP binding at the α -binding site, and that the widely open form provides an entry pathway for L-Ser with a sufficient space to reach the β -active site. Structural analyses of the simulation trajectories show that the IGP binding induces a closure of α L6 and the formation of HBs between loop 2, helix 2 of the α -subunit (α L2 and α H2, respectively, see [Figure 1A](#)), and the COMM domain. The COMM domain motions for opening the L-Ser entry pathway take place subsequently. We also show that the E(A-A) in the β -active site forms strong HBs with a portion of the COMM domain (β T110– β H115), which stabilizes a closed conformation of the COMM domain.

Table 1. Model of ApoE(Ain), IGPIE(Ain), and IGPIE(A-A) States of TRPS Used in the MD Simulations

state	PDB	α active site	β active site	modeled residues	protonated residues	initial domain structure (α/β)
ApoE(Ain)	1K8X ²⁰	none	E(Ain)	α : 178–195, 268 β : 1, 393–397	α E49	open/open
IGPIE(Ain)	1WBJ ²¹	IGP-bound	E(Ain)	α : 268 β : 392–397	α E49	closed/open
IGPIE(A-A)	2J9X ¹³	IGP-bound	E(A-A)	α : 1, 190–192 β : 397	α E49, β K87	closed/closed

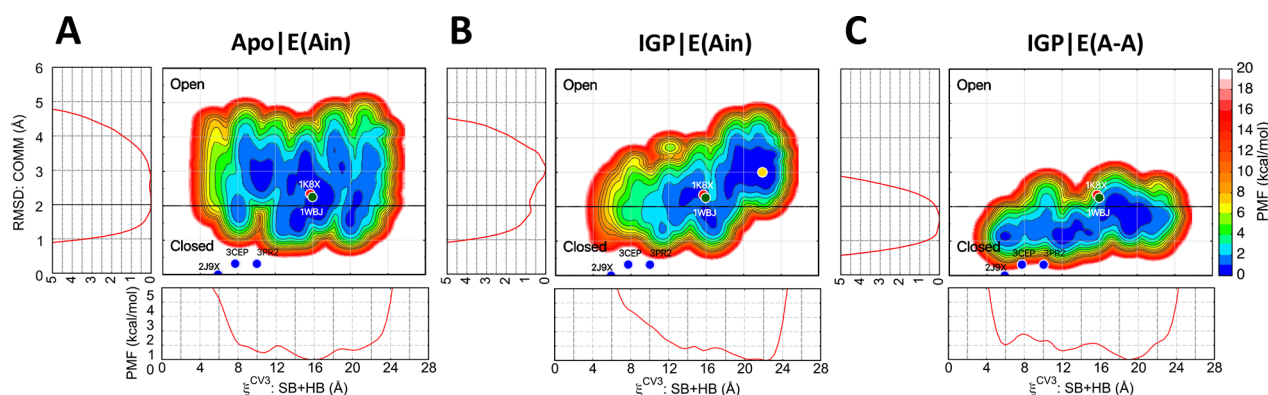


Figure 2. 2D-PMFs along ξ^{CV3} (eq 3) and the RMSD of the COMM domain in reference to an X-ray crystal structure (PDB ID: 2J9X¹³) in the ApoE(Ain) (A), IGPIE(Ain) (B), and IGPIE(A-A) (C) states. 1D-PMFs along ξ^{CV3} and RMSD are also shown in the bottom and left of each panel, respectively. X-ray crystal structures of ApoE(Ain) (PDB ID: 1K8X²⁰), IGPIE(Ain) (PDB ID: 1WBJ²¹), IGPIE(A-A) (PDB ID: 2J9X, 3CEP,⁶⁸ and 3PR2⁶⁹) states are shown in red, green, and blue circles, respectively. The yellow circle in the IGPIE(Ain) state represents a widely open COMM domain obtained in the present MD simulation.

2. COMPUTATIONAL DETAILS

2.1. System Setup. All-atom models of three different physiological states, namely, ApoE(Ain), IGPIE(Ain), and IGPIE(A-A) states were prepared based on the X-ray crystal structures; PDBID: 1K8X,²⁰ 1WBJ,²¹ and 2J9X,¹³ respectively. In the IGP bound states, the inhibitor in the α -active site was replaced manually with IGP in reference to the crystal structure, PDBID: 1QOQ.²² Cs⁺ in the monovalent cation site of 2J9X was replaced with Na⁺. The atomic structures of missing residues were modeled by GalaxyFill⁵² via CHARMM-GUI.⁵³ α L87 of 1K8X and 1WBJ was replaced to α L87 to be consistent with 2J9X. The information of all-atom models used in MD simulations is summarized in Table 1. Topology files used in the MD simulations were generated by antechamber and tleap module of AMBER18.²⁷ The force field was set to FF14SB⁵⁴ for TRPS and generalized AMBER force field 2 (GAFF2)^{55,56} for the ligands. The charges of the ligands were parametrized by quantum chemical calculations at the AM1 level. TRPS in each state was set in a cubic box of 120 × 120 × 120 Å³ with TIP3P water molecules, and the system was neutralized by 150 mM K⁺ and Cl[−] ions. All molecular graphic images were generated using Visual Molecular Dynamics (VMD)⁵⁷ and PyMOL.⁵⁸

2.2. MD Simulations. Each simulation system was first optimized with energy minimization and then equilibrated by MD simulations in several steps. The details of the equilibration steps are summarized in Tables S1 and S2. MD simulations in the NVT and NPT ensembles were carried out for 4.6 ns in the first seven equilibration steps followed by those with umbrella potentials for 11 ns in two steps. Then, the production runs of US-MD simulations were performed for 50 ns with 22 umbrella windows (1.1 μ s in total) in the NVT ensemble. The temperature and pressure were controlled at

300 K and 1 atm using the BUSSI thermostat.⁵⁹ The time step was set to 2.0 fs. Reference system propagator algorithm (RESPA)⁶⁰ was used to calculate the reciprocal-space interactions and forces every other step. The smooth particle-mesh Ewald (PME) method^{61,62} was used to calculate long-range electrostatic interactions, and the cutoff distance was set as 8.0 Å. The reaction coordinate of US-MD was defined in terms of distances of a salt bridge (SB) between β R141 and β D305 and a HB between β R141 and β S299

$$\xi^{CV1} = |\text{INH1}(R141) - \text{OD2}(D305)|. \quad (1)$$

$$\xi^{CV2} = |\text{INH2}(R141) - \text{O}(S299)|. \quad (2)$$

$$\xi^{CV3} = \xi^{CV1} + \xi^{CV2}. \quad (3)$$

The reference values of ξ^{CV1} , ξ^{CV2} , and ξ^{CV3} for each window are shown in Table S3. The force constant of the umbrella potential was set to 10.0 kcal mol^{−1} Å^{−2}. The probability distributions along ξ^{CV3} show good overlaps between neighboring histograms (see Figure S2). All bonds involving hydrogen atoms were constrained using the SHAKE/RATTLE⁶³ and SETTLE⁶⁴ algorithms. The GENESIS 2.0/β program⁶⁵ was used in all MD simulations.

2.3. Analyses. The trajectory data of the last 30 ns of the production run were used to compute the PMFs and the HB probabilities in the ApoE(Ain), IGPIE(Ain), and IGPIE(A-A) states. PMF was calculated using the MBAR⁶⁶ method implemented in GENESIS analysis tools. The probability of HBs was calculated by counting the number of HBs between α L2, α L6, α H2, and the COMM domain for each snapshot of the trajectory and weight-averaging the count number using the weight factor of each snapshot from MBAR. The HB was defined by the heavy atom distance, X–(H)–Y (X and Y represent oxygen or nitrogen), being smaller than 3.6 Å.

Tunnels from the β -active site to the surface of TRPS were analyzed using CAVER 3.0 software⁶⁷ in the ApolE(Ain), IGPI E(Ain), and IGPIE(A-A) states after the US-MD simulations. The atom of the contact point in E(A-A), i.e., C4A, was set to a starting point of the tunnel analysis. Other parameters were set to probe_radius = 1.2 or 1.8 Å, shell_radius = 3.5 Å, shell_depth = 4.0 Å, and clustering_threshold = 12.0 Å.

3. RESULTS

3.1. Conformational Changes of the COMM Domain upon Ligand Binding. To examine the motion of the COMM domain upon the α - and β -ligand bindings, we calculated two-dimensional (2D-) PMFs as a function of ξ^{CV3} (eq 3) and the root mean square deviation (RMSD) of the COMM domain. The latter was measured by aligning the β -subunit except for the COMM domain in reference to an X-ray crystal structure, PDB ID: 2J9X (IGPIE(A-A) state). X-ray crystal structures, in which the COMM domain is closed (PDB ID: 3CEP, 3PR2) and open (PDB ID: 1K8X, 1WBJ), give the RMSD value of 0.58, 0.70, 2.74, and 2.67 Å, respectively. Thus, the COMM domain is referred to as open conformation when the RMSD is larger than 2.0 Å. The resulting 2D-PMFs are shown in Figure 2. In the ApolE(Ain) state, stable structures mainly exist around $\xi^{CV3} = 16$ Å and RMSD = 2.0–3.0 Å (Figure 2A), suggesting that the COMM domain takes an open form and can hardly access a closed form. In contrast, in the IGPIE(Ain) state, the stable structure is shifted toward a region of $\xi^{CV3} = 20$ –23 Å and RMSD = 2.8–3.8 Å (Figure 2B, yellow circle), an intriguing structure newly predicted in the present MD simulation. We emphasize that the COMM domain is more widely open than that of the X-ray crystal structure of the IGPIE(Ain) state (PDB ID: 1WBJ).

To further characterize the widely open form of the IGPI E(Ain), we counted the number of cavities connecting the β -active site and the surface of β -subunit, i.e., tunnels for L-Ser to access the β -active site. The number of tunnels averaged over 10 snapshot structures is listed in Table 2 (the data of each

Table 2. Average Number of Tunnels from the β -Active Site to the Surface of β -Subunit (N_{tun}) Obtained from 10 Snapshot Structures of Each State and X-ray Crystal Structures Using a Probe Radius (r_p) of 1.2 and 1.8 Å

	ξ^{CV3}	RMSD [Å]	N_{tun} with $r_p = 1.2$	N_{tun} with $r_p = 1.8$
MD (Apol E(Ain))	16.1	2.20	1.1	0.2
MD (IGPI E(Ain))	22.4	3.13	1.1	0.7
MD (IGPIE(A-A))	18.5	1.73	0.2	0.0
X-ray (1K8X)	15.7	2.74	1	0
X-ray (1WBJ)	16.0	2.67	1	0
X-ray (2J9X)	5.89	0.00	1	0

snapshot are shown in Tables S4–S6). In the closed form of the IGPIE(A-A) state, no such tunnel is detected irrespective of the size of the probe radius. On the other hand, at least one tunnel is detected in the open form of both ApolE(Ain) and IGPIE(Ain) states with a probe radius (r_p) of 1.2 Å. However, the average number of tunnels with $r_p = 1.8$ Å is reduced to 0.2 in the open form of the ApolE(Ain) state, whereas it is kept to 0.7 in the widely open form of the IGPIE(Ain) state. The result suggests that the tunnel is wider in the IGPIE(Ain) state than

in the ApolE(Ain) state, which is consistent with the RMSD value of 3.13 and 2.20 Å, respectively. Note that the tunnel with $r_p = 1.8$ Å is absent in the X-ray crystal structures, 1K8X and 1WBJ, which are both in the open form. The entry pathway for L-Ser in the widely open form is visualized in Figure 3. The entrance is located in the vicinity of the SB pair, β D305/ β R141, and its size is sufficiently large to allow L-Ser to reach the β -active site.

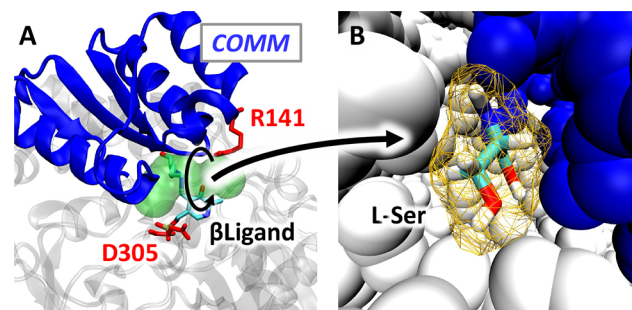


Figure 3. (A) Tunnel from the β -active site to the surface of TRPS (green) of the widely open form in the MD simulations of the IGPI E(Ain) state detected by CAVER 3.0.⁶⁷ β D305 and β R141 are shown in red, where the SB is broken in this case. (B) Smallest bottleneck radius was larger than the surface of the L-Ser (yellow wired surface). Detailed information on how to set the L-Ser in the pathway is described in the Supporting Information.

Figure 2C shows that the COMM domain is closed in the IGPIE(A-A) state. It is noticeable that the closure of the COMM domain is uncorrelated with the formation of the SB and HB. This is clearly seen in the 1D-PMF along ξ^{CV3} , where the free-energy minima are found not only around the SB/HB formation ($\xi^{CV3} = 6$ Å) but also around $\xi^{CV3} = 19$ Å. The free-energy barriers in this range are less than 1.0 kcal mol^{−1}, suggesting that the SB/HB can easily form and break while the COMM domain is kept closed.

The result so far suggests two important features. One is that the IGP binding at the α -active site induces a conformational change of the COMM domain from an open form to a widely open form. Since the α -active site and the COMM domain are spatially remote, further elucidation of the mechanism for such an allosteric regulation is intriguing. Secondly, the COMM domain is closed in the IGPIE(A-A) state, yet the formation of the SB and HB is not mandatory. Now, the question is what is the essential interaction that leads to the closure of the COMM domain? We investigate these points in the following subsections.

3.2. Wide Opening of the COMM Domain. We calculated 2D-PMFs to understand the interaction between the α L6 and the COMM domain. The first CV was set to a distance between a nitrogen atom of α G181 in α L6 and an oxygen atom of β S178, which belongs to the COMM domain,

$$\zeta(r) = |\text{N(G181)} - \text{O(S178)}|. \quad (4)$$

The previous structural studies have reported that the HB was formed between α G181 and β S178 in a closed form.²⁶ Therefore, we use this HB as a measure of the α -subunit conformation: when $\zeta < 3.75$ Å the α -subunit is referred to as a closed form. The second CV was set to the RMSD of the COMM domain, the same as in Figure 2. The result is shown in Figure 4. In the ApolE(Ain) state, both α L6 and COMM domains are in an open form sampling a wide configurational

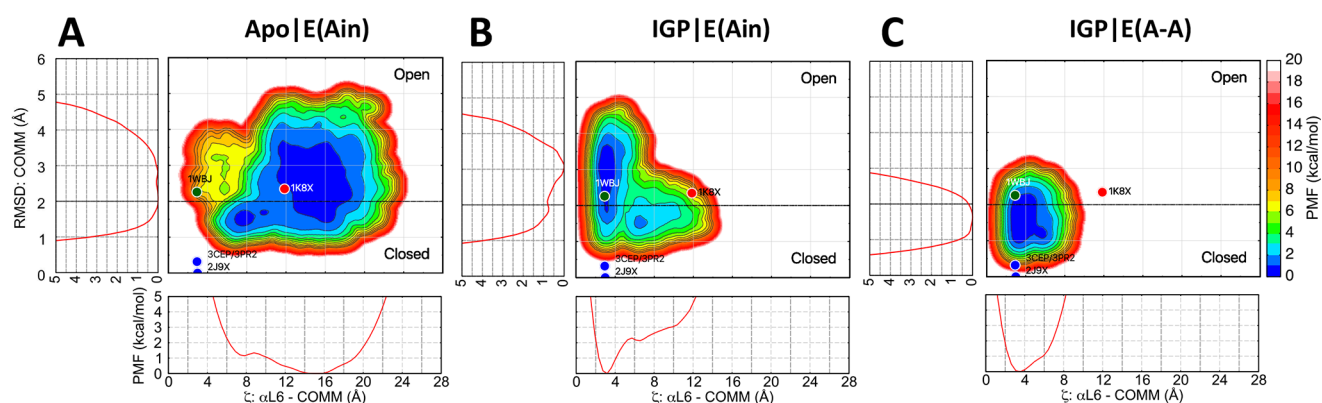


Figure 4. Two-dimensional PMFs along ζ (eq 4) and the RMSD of a COMM domain in reference to 2J9X in the ApoE(Ain) (A), IGPIE(Ain) (B), and IGPIE(A-A) (C) states. 1D-PMFs along ζ and RMSD are also shown in the bottom and left of each panel, respectively. X-ray crystal structures of ApoE(Ain) (PDB ID: 1K8X), IGPIE(Ain) (PDB ID: 1WBJ), IGPIE(A-A) (PDB ID: 2J9X, 3CEP, and 3PR2) states are shown in red, green, and blue circles, respectively.

space (Figure 4A). The stable structure is found in a region around $\zeta = 12 \sim 18$ Å and RMSD = 2.0 ~ 3.5 Å. Note that this region contains the X-ray crystal structure of the ApoE(Ain) state, 1K8X.

The IGP binding drastically changes the appearance of the 2D-PMF due to a closure of the α L6 (Figure 4B). The conformational change of α L6 is clearly observed in a 1D-PMF along ζ , which gives a deep minimum around $\zeta = 3.0$. On the other hand, the COMM domain remains in an open form but also shifts the population toward a widely open form around RMSD ~ 3.5 Å. The result suggests an allosteric communication between the α - and β -subunits, where the closure of α L6 stimulates the wide opening of the COMM domain. α L6 and COMM domains are both closed in the IGPIE(A-A) bound state (Figure 4C).

To elucidate how the α -subunit invokes the signal of IGP bindings, we focus on the change in HBs between α L2, α L6, α H2, and the COMM domain. We analyzed the probability of HB formation (p_{HB}) in the last 30 ns trajectories of the ApoE(Ain) and IGPIE(Ain) states. The results in Figure 5 show that the IGP binding triggers a growth of the HB network. The number of HBs with $p_{\text{HB}} > 0.3$ is four in the ApoE(Ain) state, whereas the number increases to six in the IGPIE(Ain) state. Furthermore, four of them are found to be strongly bound with $p_{\text{HB}} > 0.6$ (highlighted in red). Two of the strong HBs, α G61- α T183 and α G181- β S178, are visualized in Figure 6A–C. The IGP forms a HB with α D60, which induces the formation of HBs between α G61- α T183 and α G181- β S178 and the change of α L6 conformation to a closed form. Other HBs, α D60- α Q65, α Q65- β S161, and α P57- β R175, are visualized in Figure 6D,E. The HB between α D60- α Q65 changes the conformation of the α H2 (cyan allow), which recruits other HBs and shifts the COMM domain to a widely open form (blue allow). Therefore, the HB network plays an essential role in the transfer of the signal of IGP binding to the β -subunit.

Although there are mutational studies on α G181- β S178,^{25,26} no experimental study on mutation of α P57 or β R175 has been reported. To reinforce the importance of the intersubunit interaction between α P57- β R175, we mutated β R175 to β A175 and performed US-MD simulations in the same way as in the wild type (WT). The resulting 1D-PMFs along the RMSD of the COMM domain are shown in Figure 7. In the ApoE(Ain) state, the PMF of the mutant is very similar to that of WT, indicating

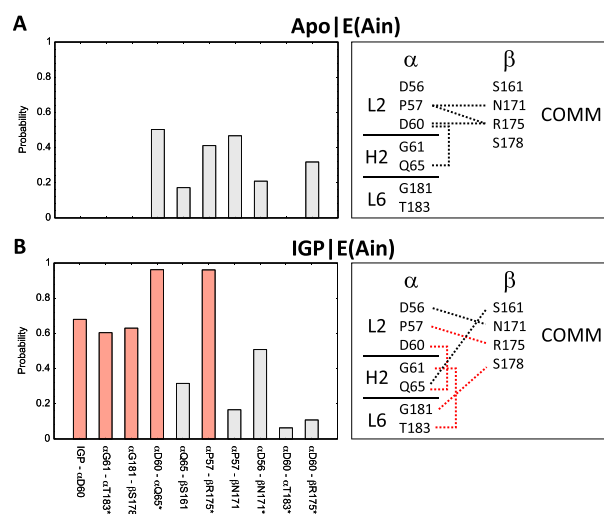


Figure 5. Probability of HB formation (left) and schematic representations of the HB network (right) in the ApoE(Ain) and IGPIE(Ain) state. The main HBs with the probability > 0.6 are shown in red color. Asterisk indicates the HBs present in the X-ray crystal structures of the IGPIE(Ain) state, 1WBJ.

that the conformation of the ApoE(Ain) state is unaffected by the mutation. In contrast, the PMF of the IGPIE(Ain) state of the mutant is different from that of the WT. The conformational change from open to widely open forms is suppressed in the mutant due to the lack of a HB between α P57- β R175.

3.3. Closure of the COMM Domain. To clarify the driving force to close the COMM domain, we analyzed the HBs between the β -subunit and the β -ligand [E(Ain) or E(A-A)] in the last 30 ns trajectories of the IGPIE(Ain) and IGPIE(A-A) states. The probability of HB formation and the structure are shown in Figure 8. Regardless of the presence of L-Ser, the phosphate group of PLP is always hydrogen-bonded with β G232- β N236. These HBs stabilize the position of PLP in the β -active site. The difference in the HB network between IGPIE(Ain) and IGPIE(A-A) states is observed in a portion of the COMM domain, β T110- β H115, which is strongly hydrogen-bonded with an aminoacrylate moiety of E(A-A). As shown in Figure 8D, these HBs largely shift the position of β T110- β H115. Note that the intersubunit HBs are kept unchanged by the closure of the COMM domain (Figure S3).

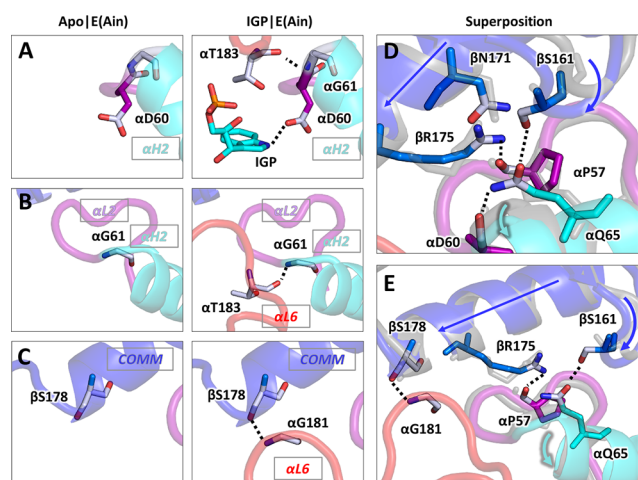


Figure 6. HB network between $\alpha L2$, $\alpha H2$, $\alpha L6$, and the COMM domain. (A–C) HBs between IGP- $\alpha D60$, $\alpha G61$ - $\alpha T183$, and $\alpha G181$ - $\beta S178$, which are present in the IGPIE(Ain) state (right) and absent in the ApoE(Ain) state (left). (D, E) HBs between $\alpha D60$ - $\alpha Q65$, $\alpha Q65$ - $\beta S161$, and $\alpha P57$ - $\beta R175$ formed in the IGPIE(Ain) state. The structure of the ApoE(Ain) state is superimposed with a transparent gray color.

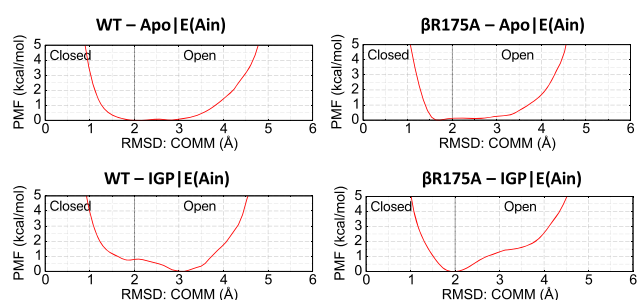


Figure 7. 1D-PMF of RMSD of COMM domain in the WT–ApoE(Ain) (top-left), $\beta R175A$ –ApoE(Ain) (top right), WT–IGPIE(Ain) (bottom left), and $\beta R175A$ –IGPIE(Ain) state (bottom right).

These results suggest that the closed form of the COMM domain is stabilized by strong HBs formed with the E(A-A) intermediate.

The remaining question is when is the COMM domain closed, i.e., upon the binding of L-Ser to the β -active site or the formation of E(A-A) after the reaction of PLP and L-Ser? To clarify this point, we have carried out an additional MD simulation after converting E(A-A) to E(Ain) and adding L-Ser [denoted E(Ain).L-Ser]. The initial structure was taken from one of the stable structures of IGPIE(A-A). After the system was equilibrated as before (see Table S1), the production run was performed for 50 ns. Figure 9 shows the time series of RMSD of the COMM domain along the simulation time. Although the RMSD is slightly increased in the initial stage, it is stabilized around 2.0 Å after 30 ns. The COMM domain does not reach a widely opened form, and L-Ser remains intact at the β -active site. The probability of HB formation and the structure of IGPIE(Ain).L-Ser are shown in Figure 10. Although the HBs with $\beta G113$ - $\beta H115$ are absent, L-Ser is strongly hydrogen-bonded with $\beta G110$ - $\beta H112$. It is plausible that these HBs prevent wide opening of the COMM domain. Therefore, we suggest that the L-Ser binding induces the conformational change of the COMM domain from widely

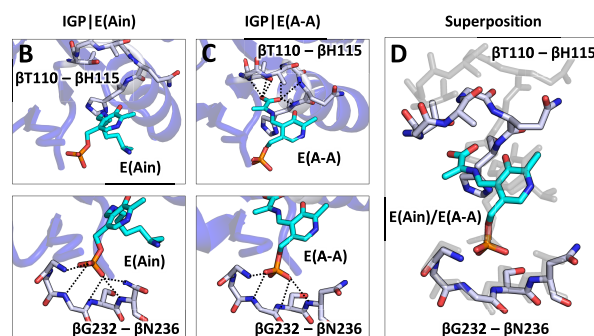
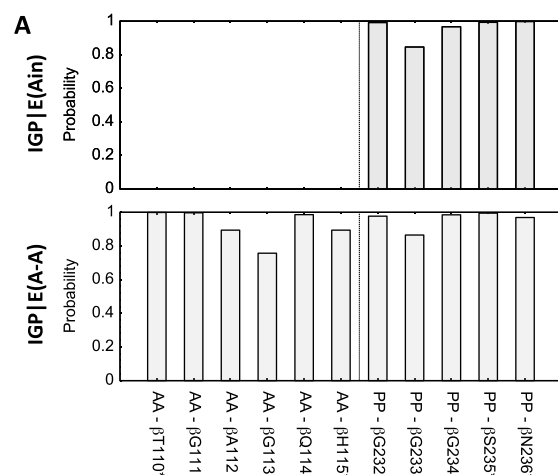


Figure 8. (A) Probability of HB formation in the IGPIE(Ain) and IGPIE(A-A) states. AA and PP indicate the α -aminoacrylate and phosphate group, respectively. Asterisk represents the HBs present in the X-ray crystal structure, 2J9X. (B, C) HBs between the β -subunit and the β -ligand in the IGPIE(Ain) and IGPIE(A-A) states. (D) Superposition of the conformation in the IGPIE(Ain) state (gray transparent) and IGPIE(A-A) state (colored) around the β -ligand. The two structures were superimposed by all C_α atoms of TRPS except for those of $\alpha L2$, $\alpha L6$, $\alpha H2$, and COMM.

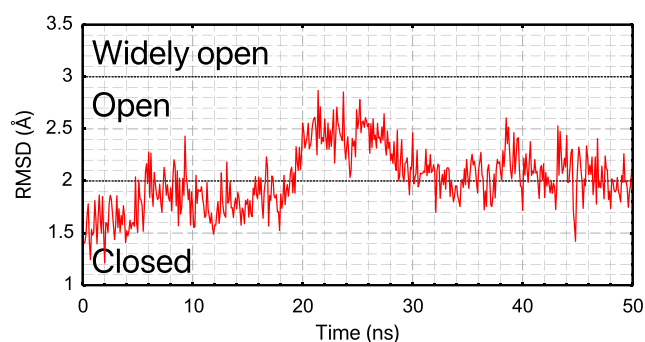


Figure 9. RMSD of the COMM domain in the IGPIE(Ain).L-Ser state.

open to open, and the COMM domain is further closed upon the formation of E(A-A).

4. DISCUSSION AND CONCLUSIONS

MD simulations of TRPS have been carried out in three ligand bound states, namely, ApoE(Ain), IGPIE(Ain), and IGPIE(A-A) states to elucidate the mechanism for the ligand-induced conformational changes of α and β -subunits. The PMF obtained from US simulations has revealed stable, widely

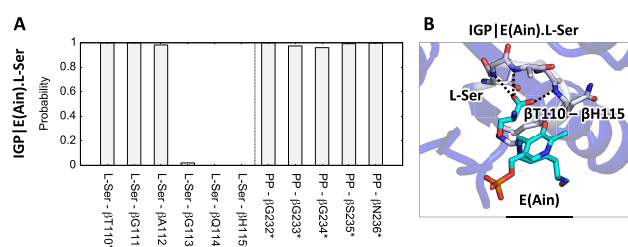


Figure 10. Probability of HB formation (A) and the structure (B) in the IGPIE(Ain).L-Ser state.

opened conformations of the COMM domain in the IGP E(Ain) state. The widely opened conformation has a sufficient space for L-Ser to enter into the β -active site, unlike the open conformation observed in X-ray crystal structures and MD simulations in ApolE(Ain) state. Such a conformational change is consistent with a kinetic experiment, which reported an increase in the binding affinity of L-Ser upon the IGP binding at the α -subunit.¹¹ In the X-ray crystal structure, the pathway for L-Ser to access the β -active site is unclear. The position/orientation of the COMM domain of the IGP E(Ain) state (PDBID: 1WBj) exhibited little change from those in the Apol E(Ain) state (PDBID: 1K8X). In another crystal structure (PDBID: 1QOQ), the COMM domain was reported to be widely opened. This structure was missing the essential monovalent cation at the β -subunit and therefore the biological meanings were not clear. The present result has clarified the entry pathway for L-Ser toward the β -active site, which passes through the SB pair (β D305 and β R141) to the β -active site (see Figure 3).

In the IGPIE(A-A) state, the α - and β -subunits are both found to be in a closed form. Although the SB between β D305 and β R141 and HB between β S299 and β R141 were suggested to play key roles in stabilizing the closed conformation of the COMM domain,⁴ the present results showed that the formation of the SB and HB is uncorrelated with the closure of the COMM domain. Instead, the present calculation suggests that the closure is driven by strong HBs between an aminoacrylate moiety of the E(A-A) intermediate and a portion of the COMM domain (β T110- β H115). The finding is in line with the very recent mutagenesis experiment of β Q114A, which observed an alternation of the stability of the open and closed conformations of the COMM domain in the mutant.²⁴

In summary, the present MD simulation has revealed the mechanism for allosteric regulation of TRPS in atomic details. (1) The IGP binding to the α -active site induces a closure of α L6, (2) the fix of α L6 stimulates the development of a HB network among α L2, α H2, α L6, and the COMM domain, (3) the intersubunit HBs, α G181- β S178 and α P57- β R175, shift the position of the COMM domain and make it widely opened to allow the entrance of L-Ser, (4) after the reaction of L-Ser and PLP, the product, E(A-A) intermediate, forms strong HBs with the COMM domain to close the conformation. In [Movie S1](#), we have summarized our findings on the relationship between α and β -ligand binding and the COMM domain opening/closure.

The present study dealt with TRPS from *Salmonella typhimurium* (St TRPS) because there are many fundamental structural data and compiled knowledge from previous experimental studies. Unfortunately, the sequence similarity between St TRPS and *M.tb* TRPS is not high, 27% and 57% for

the α and β -subunits, respectively. Therefore, the scenario may not be applicable directly to *M.tb* TRPS for TB drug design. Nonetheless, a similar computation is readily applicable to *M.tb* TRPS to identify the key site of intersubunit communication.

Although the present study focused on the conformational heterogeneity of TRPS, the atomic details on allosteric chemical reactions, namely, the enhancement of $E(\text{Ain}).\text{L-Ser} \rightarrow E(\text{A-A})$ induced by IGP binding and the activation of the α -reaction and indole transfer by the formation of $E(\text{A-A})$, remain an open question. To study the enzymatic reaction, classical molecular dynamics simulation is not enough. We need to perform hybrid QM/MM calculations of both α and β -reactions.⁷⁰ Transfer of indole from the α to β -active sites in a narrow tunnel between them provides another computational challenge for us. Without such computational effort, we consider that we are not able to fully understand molecular functions of TRPS and its allosteric regulations. Fortunately, efficient computational methods and sufficient resources are now available to answer these challenging questions.

■ ASSOCIATED CONTENT

Supporting Information


The Supporting Information is available free of charge at <https://pubs.acs.org/doi/10.1021/acs.jpcb.2c01556>.

The relationship between α and β -ligand binding and the COMM domain opening/closure (MP4)

Details on the method and calculations (Tables S1–S3) and additional data (Tables S4–S6, Figures S1–S3) ([PDF](#))

■ AUTHOR INFORMATION

Corresponding Author

Yuji Sugita – Theoretical Molecular Science Laboratory,
RIKEN Cluster for Pioneering Research, Wako, Saitama 351-
0198, Japan; Computational Biophysics Research Team,
RIKEN Center for Computational Science, Kobe, Hyogo 650-
0047, Japan; Laboratory for Biomolecular Function
Simulation, RIKEN Center for Biosystems Dynamics
Research, Kobe, Hyogo 650-0047, Japan;  [orcid.org/0000-
0001-9738-9216](https://orcid.org/0000-0001-9738-9216); Email: sugita@riken.jp

Authors

Shingo Ito – *Theoretical Molecular Science Laboratory,
RIKEN Cluster for Pioneering Research, Wako, Saitama 351-
0198, Japan*

Kiyoshi Yagi – Theoretical Molecular Science Laboratory,
RIKEN Cluster for Pioneering Research, Wako, Saitama 351-
0198, Japan;  orcid.org/0000-0003-1120-9355

Complete contact information is available at:
<https://pubs.acs.org/10.1021/acs.jpcb.2c01556>

Notes

The authors declare no competing financial interest.

■ ACKNOWLEDGMENTS

This research is partially supported by RIKEN Pioneering Research Projects (Dynamic Structural Biology/Glycolipidologue Initiative) (to Y.S.), Program for Promoting Research on the Supercomputer Fugaku (Biomolecular dynamics in a living cell (JPMXP 1020200101)/MD-driven Precision Medicine (JPMXP 1020200201)), MEXT/KAKENHI Grants No.

JP19H05645, JP21H05249 (to Y.S.) and JP20H02701 (to K.Y.). We used a computer system HOKUSAI (project ID: Q21535), provided by the RIKEN Information System Division, and Oakridge-CX and Octopus, provided by the University of Tokyo and Osaka University, respectively, (hp200098) and Fugaku supercomputer provided by RIKEN (hp210101) through the HPCI System Research Project.

REFERENCES

- (1) Consalvi, S.; Scarpecci, C.; Biava, M.; Poce, G. Mycobacterial tryptophan biosynthesis: A promising target for tuberculosis drug development? *Bioorg. Med. Chem. Lett.* **2019**, *29*, 126731.
- (2) Lott, J. S. The tryptophan biosynthetic pathway is essential for *Mycobacterium tuberculosis* to cause disease. *Biochem. Soc. Trans.* **2020**, *48*, 2029–2037.
- (3) *Global tuberculosis report 2021*; World Health Organization, 2021.
- (4) Dunn, M. F. Allosteric regulation of substrate channeling and catalysis in the tryptophan synthase holoenzyme complex. *Arch. Biochem. Biophys.* **2012**, *519*, 154–166.
- (5) Barends, T. R. M.; Dunn, M. F.; Schlichting, I. Tryptophan synthase, an allosteric molecular factory. *Curr. Opin. Chem. Biol.* **2008**, *12*, 593–600.
- (6) Wellington, S.; Nag, P. P.; Michalska, K.; Johnston, S. E.; Jedrzejczak, R. P.; Kaushik, V. K.; Clatworthy, A. E.; Siddiqi, N.; McCarren, P.; Bajrami, B.; et al. A small-molecule allosteric inhibitor of *Mycobacterium tuberculosis* tryptophan synthase. *Nat. Chem. Biol.* **2017**, *13*, 943–950.
- (7) Michalska, K.; Chang, C.; Maltseva, N. I.; Jedrzejczak, R.; Robertson, G. T.; Gusovsky, F.; McCarren, P.; Schreiber, S. L.; Nag, P. P.; Joachimiak, A. Allosteric inhibitors of *Mycobacterium tuberculosis* tryptophan synthase. *Protein Sci.* **2020**, *29*, 779–788.
- (8) Yutani, K.; Ogasahara, K.; Tsujita, T.; Kanemoto, K.; Matsumoto, M.; Tanaka, S.; Miyashita, T.; Matsushiro, A.; Sugino, Y.; Miles, E. W. Tryptophan synthase alpha subunit glutamic acid 49 is essential for activity. Studies with 19 mutants at position 49. *J. Biol. Chem.* **1987**, *262*, 13429–13433.
- (9) Hyde, C. C.; Ahmed, S. A.; Padlan, E. A.; Miles, E. W.; Davies, D. R. Three-dimensional structure of the tryptophan synthase alpha 2 beta 2 multienzyme complex from *Salmonella typhimurium*. *J. Biol. Chem.* **1988**, *263*, 17857–17871.
- (10) Dunn, M. F.; Aguilar, V.; Brzović, P.; Drewe, W. F.; Houben, K. F.; Leja, C. A.; Roy, M. The tryptophan synthase holoenzyme complex transfers indole between the α and β sites via a 25–30 Å long tunnel. *Biochemistry* **1990**, *29*, 8598–8607.
- (11) Casino, P.; Niks, D.; Ngo, H.; Pan, P.; Brzović, P.; Blumenstein, L.; Barends, T. R.; Schlichting, I.; Dunn, M. F. Allosteric regulation of tryptophan synthase channeling: The internal aldimine probed by trans-3-indole-3'-acrylate binding. *Biochemistry* **2007**, *46*, 7728–7739.
- (12) Brzović, P. S.; Ngo, K.; Dunn, M. F. Allosteric interactions coordinate catalytic activity between successive metabolic enzymes in the tryptophan synthase holoenzyme complex. *Biochemistry* **1992**, *31*, 3831–3839.
- (13) Ngo, H.; Kimmich, N.; Harris, R.; Niks, D.; Blumenstein, L.; Kulik, V.; Barends, T. R.; Schlichting, I.; Dunn, M. F. Allosteric Regulation of Substrate Channeling in Tryptophan Synthase: Modulation of the l-Serine Reaction in Stage I of the β -Reaction by α -Site Ligands. *Biochemistry* **2007**, *46*, 7740–7753.
- (14) Brzović, P. S.; Sawa, Y.; Hyde, C. C.; Miles, E. W.; Dunn, M. F. Evidence that mutations in a loop region of the α -subunit inhibit the transition from an open to a closed conformation in the tryptophan synthase holoenzyme complex. *J. Biol. Chem.* **1992**, *267*, 13028–13038.
- (15) Brzović, P. S.; Kayastha, A. M.; Miles, E. W.; Dunn, M. F. Substitution of glutamic acid 109 by aspartic acid alters the substrate specificity and catalytic activity of the β -subunit in the tryptophan synthase holoenzyme complex from *Salmonella typhimurium*. *Biochemistry* **1992**, *31*, 1180–1190.
- (16) Brzović, P. S.; Hyde, C. C.; Miles, E. W.; Dunn, M. F. Characterization of the functional role of a flexible loop in the α -subunit of tryptophan synthase from *Salmonella typhimurium* by rapid-scanning, stopped-flow spectroscopy and site-directed mutagenesis. *Biochemistry* **1993**, *32*, 10404–10413.
- (17) Schneider, T. R.; Gerhardt, E.; Lee, M.; Liang, P.-H.; Anderson, K. S.; Schlichting, I. Loop Closure and Intersubunit Communication in Tryptophan Synthase. *Biochemistry* **1998**, *37*, 5394–5406.
- (18) Jhee, K.-H.; Yang, L.-H.; Ahmed, S. A.; McPhie, P.; Rowlett, R.; Miles, E. W. Mutation of an Active Site Residue of Tryptophan Synthase (β -Serine 377) Alters Cofactor Chemistry. *J. Biol. Chem.* **1998**, *273*, 11417–11422.
- (19) Ferrari, D.; Yang, L.-H.; Miles, E. W.; Dunn, M. F. β D305A Mutant of Tryptophan Synthase Shows Strongly Perturbed Allosteric Regulation and Substrate Specificity. *Biochemistry* **2001**, *40*, 7421–7432.
- (20) Kulik, V.; Weyand, M.; Seidel, R.; Niks, D.; Arac, D.; Dunn, M. F.; Schlichting, I. On the Role of α Thr183 in the Allosteric Regulation and Catalytic Mechanism of Tryptophan Synthase. *J. Mol. Biol.* **2002**, *324*, 677–690.
- (21) Kulik, V.; Hartmann, E.; Weyand, M.; Frey, M.; Gierl, A.; Niks, D.; Dunn, M. F.; Schlichting, I. On the Structural Basis of the Catalytic Mechanism and the Regulation of the Alpha Subunit of Tryptophan Synthase from *Salmonella typhimurium* and BX1 from Maize, Two Evolutionarily Related Enzymes. *J. Mol. Biol.* **2005**, *352*, 608–620.
- (22) Weyand, M.; Schlichting, I. Crystal Structure of Wild-Type Tryptophan Synthase Complexed with the Natural Substrate Indole-3-glycerol Phosphate. *Biochemistry* **1999**, *38*, 16469–16480.
- (23) Nishio, K.; Morimoto, Y.; Ishizuka, M.; Ogasahara, K.; Tsukihara, T.; Yutani, K. Conformational Changes in the α -Subunit Coupled to Binding of the β 2-Subunit of Tryptophan Synthase from *Escherichia coli*: Crystal Structure of the Tryptophan Synthase α -Subunit Alone. *Biochemistry* **2005**, *44*, 1184–1192.
- (24) Ghosh, R. K.; Hilario, E.; Liu, Y.; Wang, Y.; Niks, D.; Holmes, J. B.; Sakhrani, V. V.; Mueller, L. J.; Dunn, M. F. Mutation of β Gln114 to Ala Alters the Stabilities of Allosteric States in Tryptophan Synthase Catalysis. *Biochemistry* **2021**, *60*, 3173–3186.
- (25) Marabotti, A.; De Biase, D.; Tramonti, A.; Bettati, S.; Mozzarelli, A. Allosteric Communication of Tryptophan Synthase: Functional and Regulatory Properties of the β S178P mutant. *J. Biol. Chem.* **2001**, *276*, 17747–17753.
- (26) Weyand, M.; Schlichting, I.; Herde, P.; Marabotti, A.; Mozzarelli, A. Crystal Structure of the β Ser178 \rightarrow Pro Mutant of Tryptophan Synthase: A “Knock-out” Allosteric Enzyme. *J. Biol. Chem.* **2002**, *277*, 10653–10660.
- (27) Lee, T.-S.; Cerutti, D. S.; Mermelstein, D.; Lin, C.; LeGrand, S.; Giese, T. J.; Roitberg, A.; Case, D. A.; Walker, R. C.; York, D. M. GPU-Accelerated Molecular Dynamics and Free Energy Methods in Amber18: Performance Enhancements and New Features. *J. Chem. Inf. Model.* **2018**, *58*, 2043–2050.
- (28) Phillips, J. C.; Braun, R.; Wang, W.; Gumbart, J.; Tajkhorshid, E.; Villa, E.; Chipot, C.; Skeel, R. D.; Kalé, L.; Schulten, K. Scalable Molecular Dynamics with NAMD. *J. Comput. Chem.* **2005**, *26*, 1781–1802.
- (29) Brooks, B. R.; Brooks, C. L.; Mackerell, A. D.; Nilsson, L.; Petrella, R. J.; Roux, B.; Won, Y.; Archontis, G.; Bartels, C.; Boresch, S.; Caffisch, A.; Caves, L.; Cui, Q.; Dinner, A. R.; Feig, M.; Fischer, S.; Gao, J.; Hodoscek, M.; Im, W.; Kuczera, K.; Lazaridis, T.; Ma, J.; Ovchinnikov, V.; Paci, E.; Pastor, R. W.; Post, C. B.; Pu, J. Z.; Schaefer, M.; Tidor, B.; Venable, R. M.; Woodcock, H. L.; Wu, X.; Yang, W.; York, D. M.; Karplus, M. CHARMM: The biomolecular simulation program. *J. Comput. Chem.* **2009**, *30*, 1545–1614.
- (30) Shaw, D. E.; Grossman, J. P.; Bank, J. A.; Batson, B.; Butts, J. A.; Chao, J. C.; Deneroff, M. M.; Dror, R. O.; Even, A.; Fenton, C. H.; et al. Anton 2: Raising the Bar for Performance and Programmability in a Special-Purpose Molecular Dynamics Supercomputer. SC '14: Proceedings of the International Conference for High Performance Computing

Networking, Storage and Analysis, New Orleans, LA, USA, Nov 16–21, 2014; IEEE Press: New Orleans, LA, USA, 2014; pp. 41–53.

- (31) Sugita, Y.; Kamiya, M.; Oshima, H.; Re, S. Replica-Exchange Methods for Biomolecular Simulations. *Methods Mol. Biol.* **2019**, *2022*, 155–177.
- (32) Zuckerman, D. M.; Chong, L. T. Weighted Ensemble Simulation: Review of Methodology, Applications, and Software. *Annu. Rev. Biophys.* **2017**, *46*, 43–57.
- (33) Valsson, O.; Tiwary, P.; Parrinello, M. Enhancing Important Fluctuations: Rare Events and Metadynamics from a Conceptual Viewpoint. *Annu. Rev. Phys. Chem.* **2016**, *67*, 159–184.
- (34) Sugita, Y.; Okamoto, Y. Replica-exchange molecular dynamics method for protein folding. *Chem. Phys. Lett.* **1999**, *314*, 141–151.
- (35) Sugita, Y.; Kitao, A.; Okamoto, Y. Multidimensional replica-exchange method for free-energy calculations. *J. Chem. Phys.* **2000**, *113*, 6042–6051.
- (36) Sugita, Y.; Okamoto, Y. Replica-exchange multicanonical algorithm and multicanonical replica-exchange method for simulating systems with rough energy landscape. *Chem. Phys. Lett.* **2000**, *329*, 261–270.
- (37) Kamiya, M.; Sugita, Y. Flexible selection of the solute region in replica exchange with solute tempering: Application to protein-folding simulations. *J. Chem. Phys.* **2018**, *149*, 72304.
- (38) Dokainish, H. M.; Sugita, Y. Exploring Large Domain Motions in Proteins Using Atomistic Molecular Dynamics with Enhanced Conformational Sampling. *Int. J. Mol. Sci.* **2021**, *22*, 270.
- (39) Oshima, H.; Re, S.; Sugita, Y. Replica-Exchange Umbrella Sampling Combined with Gaussian Accelerated Molecular Dynamics for Free-Energy Calculation of Biomolecules. *J. Chem. Theory Comput.* **2019**, *15*, 5199–5208.
- (40) Laio, A.; Parrinello, M. Escaping free-energy minima. *Proc. Natl. Acad. Sci. U. S. A.* **2002**, *99*, 12562–12566.
- (41) Bonomi, M.; Bussi, G.; Camilloni, C.; Tribello, G. A.; Banáč, P.; Barducci, A.; et al. Plumed consortium, Promoting transparency and reproducibility in enhanced molecular simulations. *Nat. Methods* **2019**, *16*, 670–673.
- (42) Yu, I.; Mori, T.; Ando, T.; Harada, R.; Jung, J.; Sugita, Y.; Feig, M. Biomolecular Interactions Modulate Macromolecular Structure and Dynamics in Atomistic Model of a Bacterial Cytoplasm. *eLife* **2016**, *5*, 18457.
- (43) Jung, J.; Nishima, W.; Daniels, M.; Bascom, G.; Kobayashi, C.; Adedoyin, A.; Wall, M.; Lappala, A.; Phillips, D.; Fischer, W.; et al. Scaling molecular dynamics beyond 100,000 processor cores for large-scale biophysical simulations. *J. Comput. Chem.* **2019**, *40*, 1919–1930.
- (44) Spyraakis, F.; Raboni, S.; Cozzini, P.; Bettati, S.; Mozzarelli, A. Allosteric communication between α and β subunits of tryptophan synthase: Modelling the open-closed transition of the α subunit. *Biochim. Biophys. Acta* **2006**, *1764*, 1102–1109.
- (45) Fatmi, M. Q.; Ai, R.; Chang, C. A. Synergistic Regulation and Ligand-Induced Conformational Changes of Tryptophan Synthase. *Biochemistry* **2009**, *48*, 9921–9931.
- (46) Fatmi, M. Q.; Chang, C. A. The Role of Oligomerization and Cooperative Regulation in Protein Function: The Case of Tryptophan Synthase. *PLoS Comput. Biol.* **2010**, *6*, No. e1000994.
- (47) Parveen, T.; Kamran, M.; Fatmi, M. Q. Structural and dynamical thermostability of psychrophilic enzyme at various temperatures: Molecular dynamics simulations of tryptophan synthase. *Arch. Biochem. Biophys.* **2019**, *663*, 297–305.
- (48) Maria-Solano, M. A.; Iglesias-Fernández, J.; Osuna, S. Deciphering the Allosterically Driven Conformational Ensemble in Tryptophan Synthase Evolution. *J. Am. Chem. Soc.* **2019**, *141*, 13049–13056.
- (49) Zhang, D.; Lazim, R. Exploring indole channeling in tryptophan synthase using steered molecular dynamics simulation. *Chem. Phys. Lett.* **2019**, *734*, 136701.
- (50) Teixeira, C. S. S.; Ramos, M. J.; Sousa, S. F.; Cerqueira, N. M. F. S. A. Solving the Catalytic Mechanism of Tryptophan Synthase: an Emergent Drug Target in the Treatment of Tuberculosis. *ChemCatChem* **2020**, *12*, 227–237.
- (51) Torrie, G. M.; Valleau, J. P. Nonphysical sampling distributions in Monte Carlo free-energy estimation: Umbrella sampling. *J. Comput. Phys.* **1977**, *23*, 187–199.
- (52) Coutsiaris, E. A.; Seok, C.; Jacobson, M. P.; Dill, K. A. A kinematic view of loop closure. *J. Comput. Chem.* **2004**, *25*, 510–528.
- (53) Jo, S.; Kim, T.; Iyer, V. G.; Im, W. CHARMM-GUI: A web-based graphical user interface for CHARMM. *J. Comput. Chem.* **2008**, *29*, 1859–1865.
- (54) Maier, J. A.; Martinez, C.; Kasavajhala, K.; Wickstrom, L.; Hauser, K. E.; Simmerling, C. ff14SB: Improving the Accuracy of Protein Side Chain and Backbone Parameters from ff99SB. *J. Chem. Theory Comput.* **2015**, *11*, 3696–3713.
- (55) Wang, J.; Wolf, R. M.; Caldwell, J. W.; Kollman, P. A.; Case, D. A. Development and testing of a general amber force field. *J. Comput. Chem.* **2004**, *25*, 1157–1174.
- (56) He, X.; Man, V. H.; Yang, W.; Lee, T.-S.; Wang, J. A fast and high-quality charge model for the next generation general AMBER force field. *J. Chem. Phys.* **2020**, *153*, 114502.
- (57) Humphrey, W.; Dalke, A.; Schulten, K. VMD: Visual molecular dynamics. *J. Mol. Graphics* **1996**, *14*, 33–38.
- (58) The PyMOL Molecular Graphics System, Version 2.5, Schrödinger: LLC, 2021.
- (59) Bussi, G.; Donadio, D.; Parrinello, M. Canonical sampling through velocity rescaling. *J. Chem. Phys.* **2007**, *126*, No. 014101.
- (60) Tuckerman, M.; Berne, B. J.; Martyna, G. J. Reversible multiple time scale molecular dynamics. *J. Chem. Phys.* **1992**, *97*, 1990–2001.
- (61) Darden, T.; York, D.; Pedersen, L. Particle mesh Ewald: An $N \log(N)$ method for Ewald sums in large systems. *J. Chem. Phys.* **1993**, *98*, 10089–10092.
- (62) Essmann, U.; Perera, L.; Berkowitz, M. L.; Darden, T.; Lee, H.; Pedersen, L. G. A smooth particle mesh Ewald method. *J. Chem. Phys.* **1995**, *103*, 8577–8593.
- (63) Andersen, H. C. Rattle: A “velocity” version of the shake algorithm for molecular dynamics calculations. *J. Comput. Phys.* **1983**, *52*, 24–34.
- (64) Miyamoto, S.; Kollman, P. A. Settle: An analytical version of the SHAKE and RATTLE algorithm for rigid water models. *J. Comput. Chem.* **1992**, *13*, 952–962.
- (65) Jung, J.; Kasahara, K.; Kobayashi, C.; Oshima, H.; Mori, T.; Sugita, Y. Optimized Hydrogen Mass Repartitioning Scheme Combined with Accurate Temperature/Pressure Evaluations for Thermodynamic and Kinetic Properties of Biological Systems. *J. Chem. Theory Comput.* **2021**, *17*, 5312–5321.
- (66) Shirts, M. R.; Chodera, J. D. Statistically optimal analysis of samples from multiple equilibrium states. *J. Chem. Phys.* **2008**, *129*, 124105.
- (67) Chovancova, E.; Pavelka, A.; Benes, P.; Strnad, O.; Brezovsky, J.; Kozlikova, B.; Gora, A.; Sustr, V.; Klvana, M.; Medek, P.; et al. CAVER 3.0: A Tool for the Analysis of Transport Pathways in Dynamic Protein Structures. *PLoS Comput. Biol.* **2012**, *8*, e1002708.
- (68) Barends, T. R. M.; Domratcheva, T.; Kulik, V.; Blumenstein, L.; Niks, D.; Dunn, M. F.; Schlichting, I. Structure and Mechanistic Implications of a Tryptophan Synthase Quinonoid Intermediate. *ChemBioChem* **2008**, *9*, 1024–1028.
- (69) Lai, J.; Niks, D.; Wang, Y.; Domratcheva, T.; Barends, T. R. M.; Schwarz, F.; Olsen, R. A.; Elliott, D. W.; Fatmi, M. Q.; Chang, C. A.; et al. X-ray and NMR Crystallography in an Enzyme Active Site: The Indoline Quinonoid Intermediate in Tryptophan Synthase. *J. Am. Chem. Soc.* **2011**, *133*, 4–7.
- (70) Yagi, K.; Ito, S.; Sugita, Y. Exploring the Minimum-Energy Pathways and Free-Energy Profiles of Enzymatic Reactions with QM/MM Calculations. *J. Phys. Chem. B* **2021**, *125*, 4701–4713.